Experiments in Fluids (2025) 66:18
https://doi.org/10.1007/s00348-024-03951-5

RESEARCH ARTICLE

Holographic focusing schlieren imaging (HFSI) for three-dimensional flow visualization

Zhiming Lin[1] · Yiqin Li[1] · Aimin Xie[2] · Kaihui Liu[1] · Zhiliang Xue[1] · Qiwen Jin[1] · Yingchun Wu[1] · Xuecheng Wu[1]

Received: 28 September 2024 / Revised: 23 November 2024 / Accepted: 20 December 2024 / Published online: 5 January 2025

Abstract

Flow field visualization techniques, e.g., schlieren and shadowgraphy, are indispensable in fluid mechanics research and application. In this paper, we present a novel technique, named holographic focusing schlieren imaging (HFSI), which takes only a single-camera and single-shot configuration to achieve three-dimensional (3D) flow visualization. The essence of this technique is that a coherent reference wave is introduced to interfere with the wavefront yielded by the traditional focusing schlieren (FS) method, forming a hologram. The reconstruction of the hologram directly yields the FS results along the test volume slice by slice with adjustable intervals, achieving 3D visualization. To demonstrate the capability of HFSI, a proof-of-concept setup was established, and experiments were performed using a compressed air jet, with a comparison to the FS method. The result shows that HFSI image reconstruction remarkably refocuses the out-of-focus jet flow, yielding similar schlieren effect observed in the FS images. The proposed HFSI holds significant practical value in some scenarios, such as in a wind tunnel, as it requires only one pair of parallel windows to achieve 3D flow visualization.

1 Introduction

Flow visualization and measurement are irreplaceable for understanding the physics of fluids that is the underlying support to the development of spacecrafts, motor vehicles, and energy conversion systems. If the structure of the flow field can be visualized, then it is also possible to get a general idea of the hydrodynamic properties of the current system and to grasp the characteristics of the flow field distribution. In general, the density of the flow field acts as a fundamental parameter that reflects its structural characteristics, and it has a close connection with the velocity, pressure, and temperature fluctuation in flows. It provides insights into many crucial aerodynamic phenomena and issues, such as shock waves, boundary layer transition, and flow separation. Consequently, diagnosing flow density is of great importance for improving structural design and optimizing the aerodynamic performance of fluid machinery.

Schlieren photography, making inhomogeneities in transparent media visible and offering intuitive visualization of flow density fluctuations that are free of post-processing, serves as a vital tool for flow diagnosis. Conventional schlieren (Settles 2001; Settles and Hargather 2017) (CS), typically referred to as Toepler's schlieren, has the merit of simplicity and ease of implementation. However, CS also has some limitations. The primary one is that it gives a line-of-sight result of the entire test volume, meaning a depth of field (DOF) on the order of the entire test width. Therefore, the flow density fluctuations are convolved with extraneous features, which also can be caused by any flaw in the surface of the collimating lenses or mirrors and the unevenness of optical windows (Weisberger and Bathel 2022). Additionally, relying on the path-integrated results is insufficient to capture the intricate details of three-dimensional (3D) flow structures such as boundary layers and turbulent shear layers. Moreover, its field of view (FOV) directly depends on the effective aperture or diameter of the collimating lenses or mirrors. This necessitates the use of lenses or mirrors of large size, with associated high cost and strict hardware requirements. Focusing schlieren (Burton 1949; Schardin 1970; Weinstein 2010; Hartmann 2021) (FS) partially addresses the drawbacks of CS in the line-of-sight effect and the FOV limitation. Making use of optical grids and a focusing lens, it has the ability to focus on a certain plane,

✉ Xuecheng Wu
wuxch@zju.edu.cn

[1] State Key Laboratory of Clean Energy Utilization, Zhejiang University, Hangzhou 310027, Zhejiang, China

[2] Ultrahigh-speed Aerodynamics Research Institute, China Aerodynamics Research and Development Center, Mianyang 621000, Sichuang, China

thereby providing results of a sharp DOF along the optical path. A DOF on the order of centimeters can be achieved in a test volume of meter-level length (Weiss and Chokani 2006; VanDercreek et al. 2010). In addition to that, the utilization of a focusing lens allows for a FOV that surpasses the effective aperture of the lens (Weinstein 1993), thereby reducing the size requirements for both the lens and optical access windows. Despite the significant improvement in focusing schlieren over conventional schlieren, it remains a two-dimensional measurement technique, which can only focus on one plane of interest (POI) at a time. Acquiring 3D results necessitates multiple scanning operations, which may take a considerable amount of time and is not suitable for transient unsteady flow measurement.

Currently, multi-view or tomographic imaging from different angles is practical for achieving 3D measurement of flow fields. Holographic interferometry (Sugawara et al. 2020; Léon et al. 2022) and tomographic particle image velocimetry (Elsinga et al. 2006; Baum et al. 2013) are the most typical examples. There are also some cases of research applying multi-view imaging in schlieren to enable 3D measurement, for example, multi-view Toepler's schlieren (Ishino et al. 2016; Li et al. 2023) and multi-view background-oriented schlieren (Atcheson et al. 2008; Nicolas et al. 2016; Liu et al. 2020) to learn 3D structure of flow field and flame. It is undeniable that such techniques have powerful multi-dimensional measurement capabilities, but they necessitate the multi-view analysis to construct accurate and high-resolution 3D information. The calibration and matching between multiple viewpoints are needed. Meanwhile, they also require the object or area under test to have an open, multi-window structure. Nevertheless, it should be mentioned that optical windows positioned along multiple axes for 3D analysis purpose are often not equipped in the measured environment of confined chamber setups, such as wind tunnels, ballistic range facilities, and combustion chamber. There is often only a single directional path or orthogonal dual optical window setup, making it difficult to arrange a multi-perspective testing system around the test area.

In contrast, single-view imaging tends to be ideal for a wider range of applicable scenarios. However, it is challenging to achieve 3D measurements with only single view. Some studies have integrated light field imaging (Ng et al. 2005) techniques into FS (Kerth et al. 2019) or background-oriented schlieren (Bichal 2015; Klemkowsky et al. 2017) methods, enabling the reconstruction of multiple schlieren images from a single recording. While the light field imaging offers 3D capabilities, its inherent limitation is the lower image resolution compared to that of a conventional camera (Hall et al. 2016). Additionally, some studies have reported the utilization of a beam splitter in the optical setup of FS (Huang et al. 2011) or the implementation of RGB color separation in image processing (Martínez-González et al. 2021) to enable multiplane analysis simultaneously. However, their capacity for improvement is very limited, with upgrades to only two or three planes.

Overall, it is evident that 3D measurement of flow fields using single-view schlieren-based techniques remains feasible. In particular, FS demonstrates excellent two-dimensional capability to image a region of narrow DOF. By combining FS with 3D analytical techniques, it is possible to achieve 3D imaging for flow field measurement. Earlier studies have reported the combination of FS and holography to achieve 3D recording by single image (Weinstein 1991; Doggett and Chokani 1993; Weinstein 2010). In the proposed device structure, holographic recording and reconstruction were performed separately. A physical holographic dry plate was used as the recording medium for capturing holograms, and reconstruction was achieved by introducing a reconstruction beam to illuminate the dry plate. By adjusting the image plane, FS results corresponding to different planes within the measurement volume could be obtained. With advancements in digital holography, it has become evident that this physical recording medium can be replaced by digital recording, significantly enhancing the reusability and convenience of the device. Furthermore, in the earlier setup, holograms were recorded before the focusing lens, which posed limitations for achieving large field-of-view recordings, as the rear focusing lens can scale the light field and enable broader observation. Additionally, the separated structure of the setup may pose challenges in aligning the cutoff grid with the source grid image, potentially reducing sensitivity. To this end, in this article, we propose a novel method, named digital holographic focusing schlieren imaging (HFSI), which combines the FS and holography method to achieve 3D flow visualization by single image. The principles of HFSI are introduced, followed by a detailed description of the optical configuration. Next, the proof-of-concept experiments are conducted on static transparent capillary tubes and two spatially offset jet flows. By comparing the results obtained through FS, the imaging quality and flow visualization performance of HFSI are then discussed.

2 Concept

In an FS system, the focusing schlieren effect arises from the spatial modulation of light by the source grid and the cutoff grid. Initially, the source grid spatially modulates the incoming light. The modulated light is then projected through an imaging lens onto the cutoff grid, which blocks portions of the source grid's light based on its relative alignment with the source grid's image. The FS image of certain POIs can be obtained by moving the recording screen forward and backward along the optical axis, and the POI position can

be easily determined by the law of lens imaging. As shown in Fig. 1, establishing a Cartesian coordinate system (x, y, z) with the z axis representing the direction of the optical axis, the intensity of the resulting FS image $I_z(x, y)$ satisfies the following relationship with flow density gradient and system parameters (Settles 2001; Weinstein 1993; Cook and Chokani 1993).

$$\frac{I_z(x,y)-I_{z,0}(x,y)}{I_{z,0}(x,y)}=\frac{\Delta I_z(x,y)}{I_{z,0}(x,y)}\propto\frac{Kf}{a(L-f)}\int_{z_1}^{z_2}(L-l)\sigma(z)\frac{\partial\rho}{\partial y}\mathrm{d}z, \tag{1}$$

where $I_z(x, y)$ and $I_{z,0}(x, y)$ represent the intensity of schlieren image in the presence and absence of flow disturbances, respectively. K denotes the Gladstone–Dale coefficient for flow medium, a is the unobstructed height of the bright line of the source grid image onto the cutoff grid, and f is the focal length of the focusing lens. L and l are the distance from the source grid to the focusing lens and the distance from the POI to the focusing lens, respectively. $\sigma(z)$ is a spread function of the investigated measurement volume, while z_1 and z_2 refer to locations along the direction of z-axis where the light enters and leaves the measurement volume, respectively. When the line direction of both grids is along the x-axis direction, the density gradient along the y-axis $\partial\rho/\partial y$ can be resolved.

A key point to consider is that the light passing through the cutoff grid retains all pertinent information regarding flow density gradients in test volume. Therefore, if the wavefront of the light is recorded, the optical propagation calculation can be applied to reconstruct the light field along the optical axis. This implies that a single-shot recording of wavefront is sufficient to acquire the FS image at various POI positions. Holography is an ideal approach to record the wavefront of light. Based on the above mechanism, a schematic of the concept is shown in Fig. 2. In the proposed HFSI, a reference wave is introduced to interfere with the wavefront of the FS signal. The optical configuration involves two arms: an FS arm that generates the primary FS signal and a reference arm that generates the interfering wave. The object wave (FS signal) and reference wave are finally merged through a prism cube and recorded by the sensor, which forms an off-axis holographic system. The resulting hologram intensity is given by

$$\begin{aligned}H(x,y)&=[\mathbf{O}(x,y)+\mathbf{R}(x,y)]^2=|\mathbf{O}(x,y)|^2+|\mathbf{R}(x,y)|^2\\&+\mathbf{R}^*(x,y)\mathbf{O}(x,y)+\mathbf{R}(x,y)\mathbf{O}^*(x,y),\end{aligned} \tag{2}$$

where $H(x, y)$ is the intensity of the hologram, $\mathbf{O}(x, y)$ is the object wave, and $\mathbf{R}(x, y)$ is the reference wave that is normally known, such as a plane wave or a spherical wave.

According to Eq. 2, after performing spectrum separation in the frequency domain, this wavefront $\mathbf{O}(x, y)$ can be extracted. Then, by performing optical propagation calculations (Collier 2013) on the wavefront, it is possible to obtain

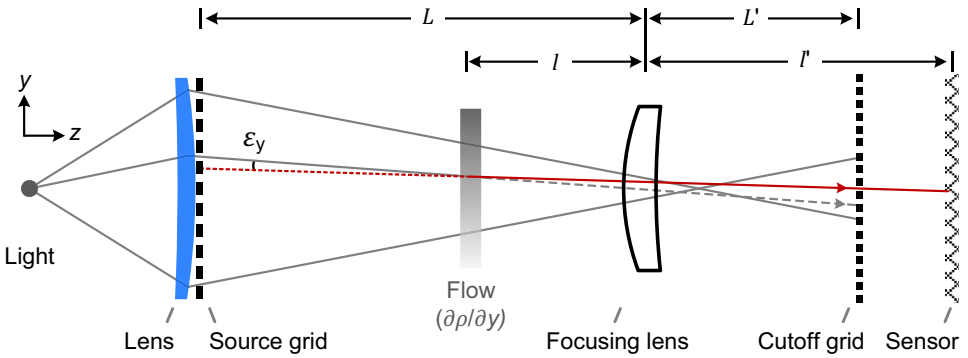

Fig. 1 Conceptual schematic of FS. The light is deflected as it passes through a region of the flow field where the refractive index changes. The solid red line is the path of the deflected ray, and the dashed red line is the inverse extension of the deflected ray path. ϵ_y is the angle between the line of extension and the ray of emission. $\partial\rho/\partial y$ denotes the gradient of the flow field density in the y-direction

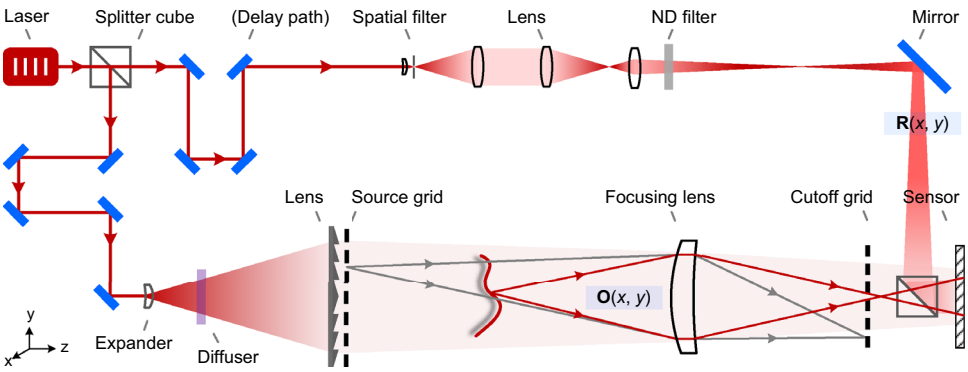

Fig. 2 Conceptual schematic of HFSI. $\mathbf{O}(x, y)$ represents the object wave, which is the wavefront of the FS signal. $\mathbf{R}(x, y)$ denotes the reference wave, typically a known plane wave or a spherical wave

the light field intensity at various positions in space, which corresponds to the FS result of different POI.

$$I_z(x,y) = \left[\mathbf{R}^*(x,y)\cdot\mathbf{O}_z(x,y)\right]^2, \tag{3}$$

where $I_z(x,y)$ represents the intensity of FS image at z and $\mathbf{O}_z(x,y)$ is the wavefront at z after the optical propagation calculation. Therefore, HFSI enables the inversion of FS images at different positions in 3D space using a single image.

The holographic reconstruction method used in our study is angular spectrum method, which can be formulated as follows

$$\mathbf{O}(x,y) = \mathcal{F}^{-1}\left\{\mathcal{F}\left[\mathbf{O}(x_0,y_0)\right]\cdot H\left(f_x,f_y\right)\right\}, \tag{4}$$

$\mathbf{O}(x_0,y_0)$ is the initial wavefront, and $H\left(f_x,f_y\right)$ is the transfer function of the system in the frequency domain. $\mathcal{F}$ and $\mathcal{F}^{-1}$ denote the Fourier forward and Fourier inverse transforms, respectively. $H\left(f_x,f_y\right)$ can be expressed as

$$H\left(f_x,f_y\right) = \exp\left[\mathrm{i}\cdot kz\cdot\sqrt{1-\left(\lambda f_x\right)^2-\left(\lambda f_y\right)^2}\right], \tag{5}$$

where i is the imaginary unit, k is the wave number, and z is the interested position, λ is the wavelength. f_x and f_y are the frequency domain coordinates, respectively.

3 System

An HFSI system was designed and built in order to demonstrate the capabilities of the proposed system. The present system uses a pulsed laser with a wavelength of 532 nm and a pulse width of 0.5 ns as the illumination source. The laser beam is split into two beams with an intensity ratio of 1 to 9, serving as the light source for the reference arm and the FS arm, respectively. There were two delay paths to ensure the interference of two beams. Subsequently, the beam transmitted through the splitter cube is filtered by a spatial filter and adjusted using a set of thin lens, forming a spherical wave as the reference wave. It is then redirected by a mirror and a splitter onto the camera. The beam reflected by the first splitter passes through an expander and is converged onto the focusing lens by a large Fresnel lens with a diameter of 100 mm and a focal length of 250 mm. To achieve uniform illumination intensities and minimize diffraction effects, a ground glass diffuser is utilized to diffuse the light beam prior to the large lens. Then the light is spatially modulated by a source grid. After that, an image of the source grid is projected through the focusing lens onto the cutoff grid, and the region of interest is imaged onto the camera by the focusing lens. As a result, the interference between the reference wave and the object wave generates a hologram on the camera. The focusing lens has a focal length f_{F} of 275 mm and a clear aperture A_{F} of 40 mm. The camera has a pixel size of 3.2 μm × 3.2 μm and a resolution of 9344 × 7000, resulting in a sensor size of 29.9 mm × 22.4 mm. The camera exposure time is set to 250 μs, while its effective exposure time is actually determined by the pulse width of the pulsed laser, which is 0.5 ps.

Two proof-of-concept experiments were conducted separately for out-of-focus static transparent capillary tubes and two spatially offset jet flows. To enable an intuitive understanding of the reconstruction quality of HFSI, the FS images were captured with each tube appearing in focus by repositioning the camera, under identical optical component arrangements. These images served as the ground truth for our assessment. Moreover, apart from the pulsed laser, a high-power continuous LED is also utilized as the illumination source to obtain FS images. The camera's exposure time is set to 100 μs. Both of the results from the pulsed laser and high-power LED illumination are used for comparison.

4 Results

The reconstruction quality of HFSI image was first investigated using transparent capillary tubes located at out-of-focus positions relative to the camera sensor position, as shown in the upper right of Fig. 3. In this study, the source grid and the cutoff grid were positioned at the conjugate plane of the lens, with magnification of 1. The height of both the source and cutoff grid's transparent and opaque stripe is are 1 mm. The capillary tube has an outer diameter of 0.5 mm, and it produces a schlieren effect with a bright center and darker edges. Figure 3 gives the comparison between the HFSI and the FS. The top row shows the defocused positions of the three tubes. The first, second, and third tubes are 10 mm, 22 mm, and 34 mm away from the plane of focus, respectively. The second row displays the reconstruction results of the HFSI image, refocused on the POI containing capillary tubes. The next two rows showcase the FS images focusing on the capillary tubes at different positions, captured under the illumination of the pulsed laser and the LED, respectively.

The HFSI images in Fig. 3 recorded the out-of-focus capillary tubes. Defocus blurs and obscures the capillary tubes in the raw HFSI images. Despite this, in the second row of Fig. 3, HFSI image reconstruction remarkably refocuses the capillary tubes, yielding results that have a similar schlieren effect observed in the FS images. However, the contrast between the reconstructed schlieren pattern of the target capillary and the background remains slightly lower compared to the FS image. Compared to the results obtained with an LED light source, the FS images and HFSI reconstructed images exhibit speckle noise, which is attributed

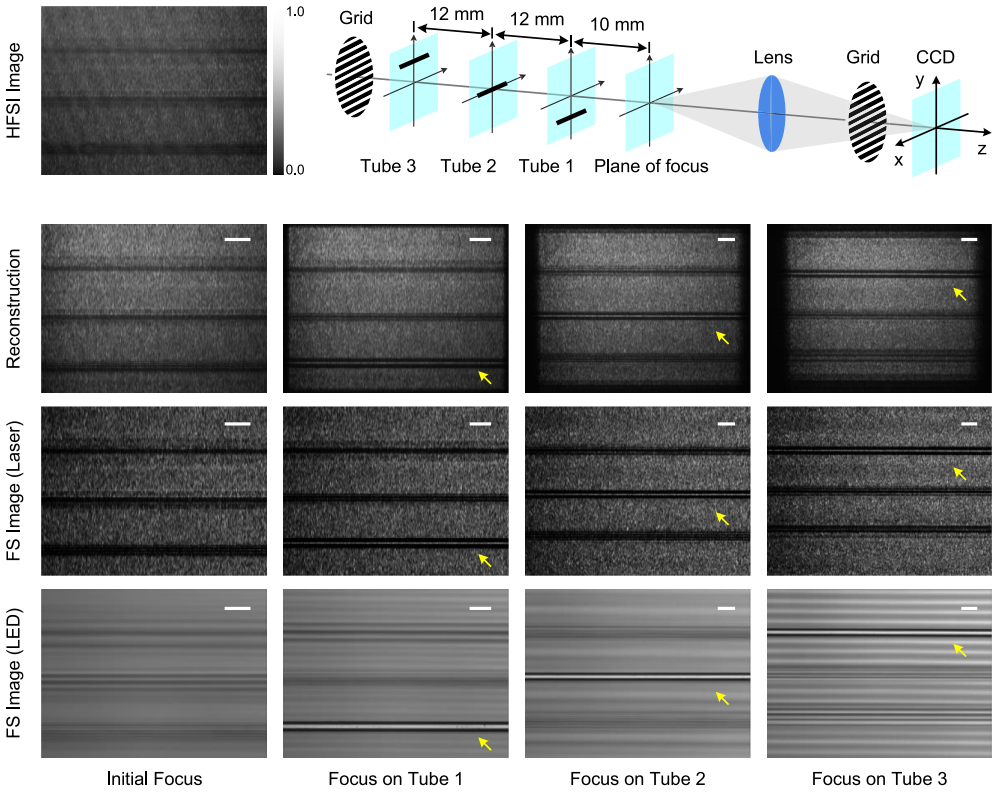

Fig. 3 From top to bottom, the first row shows the original HFSI image, the CCD, and the positions of the four examined planes; the second row shows the corresponding results when the HFSI image is reconstructed to these four positions; the third and fourth rows are the results when the camera is focused on the four positions under the laser source and the LED light source, respectively. Three tubes are 10 mm, 22 mm, and 34 mm away from the initial plane of focus. (Scale bar: 1 mm)

to the use of a laser as the illumination source. However, at the same time, we can notice that the residual shadow of the source grids in the image is significantly reduced when using the laser source.

Highlighting HFSI's 3D ability, Fig. 4 presents another experiment in which two spatially offset jet flows are located 20 mm and 55 mm away from the initial plane of focus. In this experiment, the imaging magnification is 0.5. The height of the source grid's transparent and opaque stripe is 2 mm and 1 mm, respectively. Accordingly, for the cutoff grid, they are 0.5 mm and 1 mm, respectively. The compressed air jet was chosen for the experiments, as it can generate flow with prominent density gradients, making it ideal for schlieren visualization. The outlet diameter of the nozzle was 1.5 mm. To ensure a clear schlieren effect with both pulsed laser and LED illumination, the laminar-to-turbulent transition stage of the jet is selected for observation, as it offers low flow speed and less motion blur in the case of LED light sources. As can be seen in Fig. 4, the flow remains laminar in a region downstream of the nozzle outlet of 1 to 2 times the nozzle diameter, and it develops into a turbulent state after that. In this section, the data processing of HFSI consists of holographic reconstruction, background subtraction, and image contrast enhancement. Firstly, holographic reconstruction is performed on the HFSI image using the angular spectrum method of diffraction calculation, resulting in focusing schlieren images at different depth positions z. After that, an HFSI image is recorded with a no flow background, and its reconstructed result is then subtracted from the flow on HFSI images. Finally, the histogram equalization method is used to enhance image contrast. FS images are processed in the same way as HFSI images except that holographic reconstruction is not required.

This complex flow scenario challenges traditional FS methods but HFSI effortlessly resolves the individual jet structures by a single image, showcasing its remarkable ability to visualize flow dynamics across multiple depths. Likewise, the FS image at the position of the HFSI recording position, POI of jet 1, and POI of jet 2 were also captured for comparison. As shown in the first and second column of the FS results in Fig. 4, both of the jet flows are out-of-focus in the initial position. At this point, the outline of jet 1 can be roughly observed, while jet 2 is completely blurred. By shifting the position of recording plane, each jet can be individually identified at its respective focus position. However, this requires readjustment of the sensor plane. In contrast, in the case of HFSI, the two

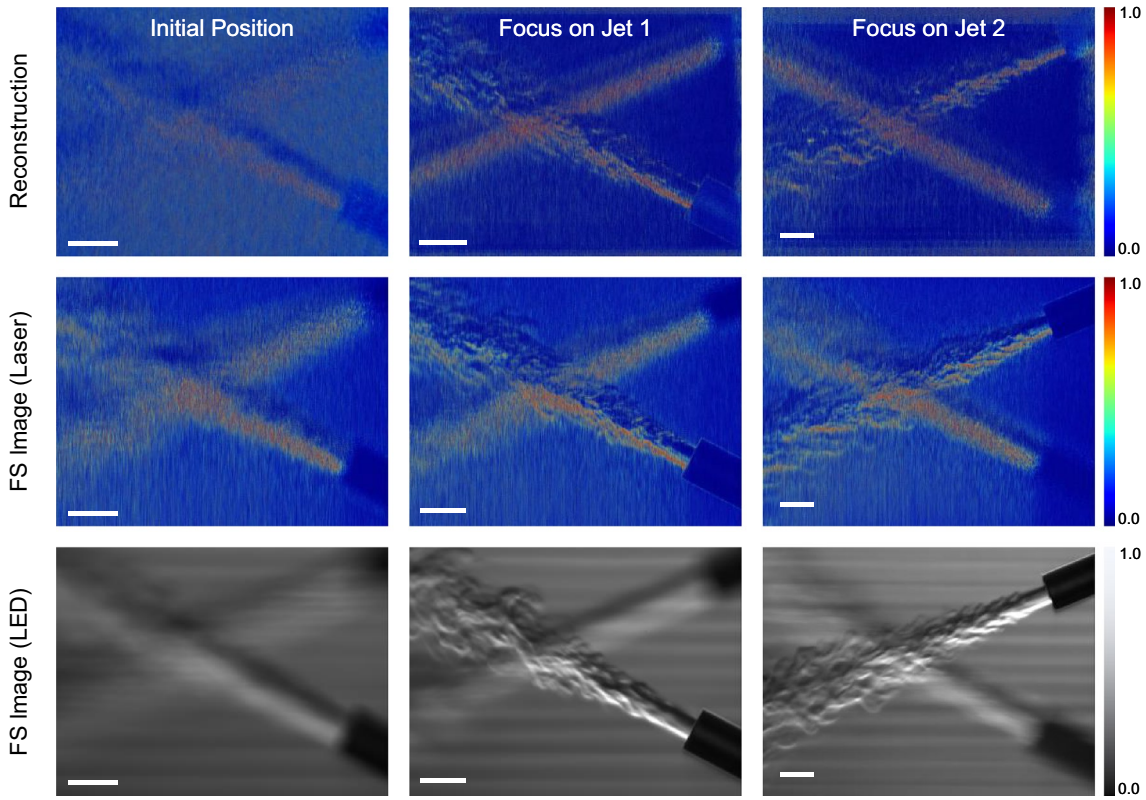

Fig. 4 From top to bottom, each row represents HFSI's reconstruction, FS image using laser illumination, and FS image using LED illumination, respectively. Two jets are located 20 mm and 55 mm away from the initial plane of focus. (Scale bar: 3 mm)

jet flows can be sharply refocused by choosing different reconstruction distances. Each reconstructed image distinguishes and separates the individual jet flows, as shown in the third column of Fig. 4, and the images obtained at both focusing planes are similar to the FS results. This depth-tunable reconstruction feat gives HFSI the potential for visualizing the interaction behaviors and dynamics of multi-depth flows that remain hidden to traditional FS methods.

It should be pointed out that the HFSI's reconstruction and the FS image obtained using the laser are of poor quality regarding visualization and sensitivity, compared to the results from the LED (exposure time 100 μs). There are significant speckles appearing in the resulting image due to the coherence of the laser and the characteristics of the diffuser. All of them reveal the same jet flow structure; the FS image by LED provides better recognition of the turbulent eddy structures.

5 Conclusion

In summary, the principle of HFSI was described in this study, and experiments are performed using a proof-of-concept setup to showcase its capabilities. HFSI image reconstruction refocuses the out-of-focus targets, achieving a level of detail comparable to the schlieren effect observed in the FS image. HFSI's 3D capability improves flow field analysis. Unlike traditional FS method requiring multiple scans to capture 3D flow dynamics at different depths, HFSI enables investigation of the entire test volume in a single recording, boosting efficiency and, more importantly, providing the ability to analyze the complex correlations between multi-depth transient flow features. From a practical standpoint, the proposed HFSI holds significant value in the scenarios, in which optical windows positioned along multiple axes for 3D analysis purposes may be impractical, such as in wind tunnels, as it requires only one pair of parallel windows for 3D flow visualization. However, it should be mentioned that the laser illumination inevitably introduces speckle noise, significantly degrading image quality and obscuring fine details. Mitigating this effect is crucial for future research on HFSI.

Funding This work was supported by the National Natural Science Foundation of China (No. 52406209), the National Natural Science Foundation of China (No. 52276167), and the Fundamental Research Funds for the Central Universities (No. 2022ZFJH004).

Data availability Data underlying the results presented in this paper are not publicly available at this time but may be obtained from the authors upon reasonable request.

Declarations

Conflict of interest The authors declare no conflict of interest.

References

Atcheson B, Ihrke I, Heidrich W, Tevs A, Bradley D, Magnor M, Seidel H-P (2008) Time-resolved 3d capture of non-stationary gas flows. ACM Trans Graph (TOG) 27(5):1–9

Baum E, Peterson B, Surmann C, Michaelis D, Bohm B, Dreizler A (2013) Investigation of the 3D flow field in an IC engine using tomographic PIV. Proc Combust Inst 34(2):2903–2910

Bichal A (2015) Development of 3D Background Oriented Schlieren with a Plenoptic Camera. PhD thesis, Auburn University

Burton RA (1949) A modified schlieren apparatus for large areas of field. J Opt Soc Am 39(11):907–908

Collier R (2013) Optical holography. Elsevier, Amsterdam

Cook S, Chokani N (1993) Quantitative results from the focusing schlieren technique. In: 31st Aerospace sciences meeting

Doggett GP, Chokani N (1993) Large-field laser holographic focusing schlieren system. J Spacecr Rocket 30(6):742–748

Elsinga GE, Scarano F, Wieneke B, Oudheusden BW (2006) Tomographic particle image velocimetry. Exp Fluids 41:933–947

Hall EM, Thurow BS, Guildenbecher DR (2016) Comparison of three-dimensional particle tracking and sizing using plenoptic imaging and digital in-line holography. Appl Opt 55(23):6410–6420

Hartmann J (2021) The acoustic air-jet generator. Technical translation (2021) NASA-TT-20210016495, Technical University of Denmark (1940)

Huang S, Xie A, Hanchen B (2011) Research on the application of two-plane focusing schlieren technology. J Exp Fluid Mech 25:92–96

Ishino Y, Hayashi N, Bt Abd Razak IF, Kato T, Kurimoto Y, Saiki Y (2016) 3D-CT (computer tomography) measurement of an instantaneous density distribution of turbulent flames with a multi-directional quantitative schlieren camera (reconstructions of high-speed premixed burner flames with different flow velocities). Flow Turbul Combust 96:819–835

Kerth P, Hermann T, McGilvray M (2019) Three-dimensional focusing schlieren using a plenoptic camera. In: International conference on flight vehicles, aerothermodynamics, re-entry missions and engineering. ESA Conference Bureau

Klemkowsky JN, Fahringer TW, Clifford CJ, Bathel BF, Thurow BS (2017) Plenoptic background oriented schlieren imaging. Meas Sci Technol 28(9):095404

Léon O, Donjat D, Olchewsky F, Desse J-M, Nicolas F, Champagnat F (2022) Three-dimensional density field of a screeching under-expanded jet in helical mode using multi-view digital holographic interferometry. J Fluid Mech 947:36

Li X, Lei Q, Bao W, Li X, Fan W (2023) Fiber-based high-speed 3D schlieren imaging. Opt Lett 48(15):4081–4084

Liu H, Shui C, Cai W (2020) Time-resolved three-dimensional imaging of flame refractive index via endoscopic background-oriented Schlieren tomography using one single camera. Aerosp Sci Technol 97:105621

Martínez-González A, Moreno-Hernández D, Guerrero-Viramontes JA, Zamarripa-Ramírez JCI, Carrillo-Delgado C (2021) Multiplane temperature measurement of fluid flows using a color focusing schlieren system. Opt Laser Technol 142:107256

Ng R, Levoy M, Brédif M, Duval G, Horowitz M, Hanrahan P (2005) Light field photography with a hand-held plenoptic camera. Technical report CSTR 2005-02

Nicolas F, Todoroff V, Plyer A, Le Besnerais G, Donjat D, Micheli F, Champagnat F, Cornic P, Le Sant Y (2016) A direct approach for instantaneous 3D density field reconstruction from background-oriented schlieren (BOS) measurements. Exp Fluids 57:1–21

Schardin H (1970) Schlieren methods and their applications. Technical Translation (1970) NASA-TT-F12731, National Aeronautics and Space Administration (1942)

Settles GS (2001) Schlieren and shadowgraph techniques: visualizing phenomena in transparent media. Springer, Berlin

Settles GS, Hargather MJ (2017) A review of recent developments in schlieren and shadowgraph techniques. Meas Sci Technol 28(4):042001

Sugawara S, Nakao S, Miyazato Y, Ishino Y, Miki K (2020) Three-dimensional reconstruction of a microjet with a Mach disk by Mach-Zehnder interferometers. J Fluid Mech 893:25

VanDercreek C, Smith M, Yu K (2010) Focused schlieren and deflectometry at AEDC hypervelocity wind tunnel No. 9. In: 27th AIAA aerodynamic measurement technology and ground testing conference

Weinstein LM (1991) An improved large-field focusing schlieren system. In: 29th Aerospace sciences meeting. Aerospace Sciences Meetings

Weinstein LM (1993) Large-field high-brightness focusing schlieren system. AIAA J 31(7):1250–1255

Weinstein L (2010) Review and update of lens and grid schlieren and motion camera schlieren. Eur Phys J Spec Top 182:65–95

Weisberger JM, Bathel BF (2022) Single source/cutoff grid, self-aligned focusing schlieren system. Exp Fluids 63:38

Weiss J, Chokani N (2006) Integration properties of the focusing schlieren deflectometer. In: 25th AIAA aerodynamic measurement technology and ground testing conference